Unimolecular Reactivity of Protonated α,ω-Alkanediamines in the Gas Phase

Guy Bouchoux,*,† Nadège Choret,† Florence Berruyer-Penaud,‡ and Robert Flammang§

Département de Chimie, Laboratoire des Mécanismes Réactionnels, UMR CNRS 7651, Ecole Polytechnique, 91128 Palaiseau Cedex, France, Laboratoire de Chimie Physique, Groupe de Chimie Théorique, UMR CNRS 8000, Bâtiment 490, Université Paris Sud, 91405 Orsay Cedex, France, and Laboratoire de Chimie Organique, Université de Mons-Hainaut, 20 Place du Parc, B-7000, Mons, Belgium

Received: April 24, 2001; In Final Form: July 9, 2001

Unimolecular deamination of protonated α,ω-alkanediamines (1,2-ethanediamine (**1**), 1,3-propanediamine (**2**), 1,4-butanediamine (**3**), and 1,5-pentanediamine (**4**)) in the gas phase has been examined by tandem mass spectrometry experiments including metastable ions decompositions and collisional activation techniques and molecular orbital calculations up to the G2(MP2,SVP) level. For all the protonated molecules, only one unimolecular dissociation channel, leading to the formation of a protonated cyclic amine via an internal nucleophilic substitution, was detected. The hydride ion transfer from the α carbon to the ω position is not competitive with the internal nucleophilic substitution. This has been found to be the result of a large critical energy for this latter reaction.

1. Introduction

α,ω-Alkanediamines are compounds of interest in various domains of organic and organometallic chemistry. They are known as chelating bidentate ligands in coordination chemistry, as reactants in industrial polymerization processes, and as synthetic enzymes for complex formations with substrates by hydrogen bonding.[1] Internal hydrogen bonding in the neutral and in the protonated forms play an important role in the conformational equilibrium of such species and consequently in their chelating ability. Gas phase protonation energetics of the first members of the series of α,ω-alkanediamines has been studied experimentally[2] and theoretically,[3] demonstrating a clear enhancement of the gas phase basicities of these molecules with respect to primary amines of comparable polarizability. This has been explained by the formation of a strong internal hydrogen bond in the protonated forms of the diamines, a proposal which has been corroborated by the observation[2] and the calculation[3] of an entropy loss upon protonation.

Besides these structural and energetic aspects, protonation of one of the amino groups of α,ω-alkanediamines is also expected to activate the corresponding C−N bond. Accordingly, the unimolecular reactivity of these protonated molecules seems to be controlled by this phenomenon since a loss of ammonia is generally observed.[4] Surprisingly enough, no information concerning the structure of the product ions and, a fortiori, the reaction mechanism of this deamination process is presently available. The goal of the present study is consequently to examine, both experimentally and theoretically, the behavior of the four simplest α,ω-alkanediamines: 1,2-ethanediamine (**1**), 1,3-propanediamine (**2**), 1,4-butanediamine (**3**), and 1,5-pentanediamine (**4**). By comparison with the homologous diols,[5] the deamination reactions of protonated α,ω-alkanediamines are expected to lead either to a protonated cyclic amine by intramolecular nucleophilic substitution (channel a, Scheme 1)

SCHEME 1

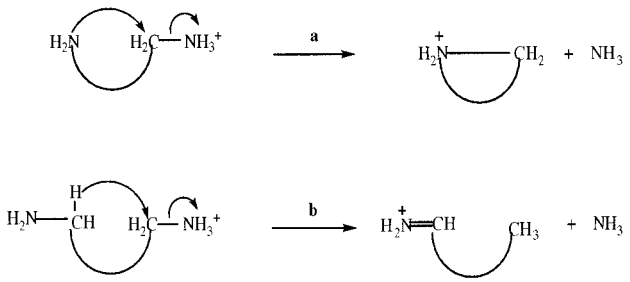

or to a protonated imine by internal hydride ion transfer (channel b, Scheme 1). This latter reaction is the unique process followed by protonated 1,2-ethanediol (the so-called "pinacol rearrangement").[5]

Tandem mass spectrometry experiments and, particularly, collisional activation may be used to characterize the structure of the ionic products of the deamination reactions. On the other hand, calculation of the potential energy profiles also provides clues to the feasibility of reactions a and b. This double approach has been applied to the ammonia loss from protonated α,ω-alkanediamines **1**−**4**. Collisional experiments were conducted in a six-sector magnetic instrument. The potential energy of each reaction path has been investigated at the MP2/6-31G(d)+ZPE level of theory; critical points have been calculated using the G2(MP2,SVP) method.

2. Experimental and Computational Section

The reactions of metastable protonated diamines were studied with a VG-ZAB-2F double focusing mass spectrometer (B-E) operating in the chemical ionization mode using methanol as reagent gas. The accelerating voltage was set at 8 kV, the electron energy at 150 eV, and the emission current at 0.5 mA. The source temperature was kept at 180 °C. The Mass analyzed Ion Kinetic Energy (MIKE) spectra of metastable ions were

† Ecole Polytechnique.
‡ Université Paris Sud.
§ Université de Mons-Hainaut.

10.1021/jp0115446 CCC: $20.00
Published on Web 09/13/2001

TABLE 1: Calculated G2(MP2,SVP) and Experimental Heats of Formation of Protonated Diamines 1−4 and Their Possible Deamination Products (kJ·mol^{-1})

species	G2(MP2,SVP) 0 K	G2(MP2,SVP) 298 K	exptl	deviation
protonated 1,2-diaminoethane, **1H**$^+$	599.5	566.1	562.6[a]	−3.5
protonated 1,3-diaminopropane, **2H**$^+$	557.9	517.3	513.6[a]	−3.7
protonated 1,4-diaminobutane, **3H**$^+$	525.9	478.3	479.7[a]	1.4
protonated 1,5-diaminopentane, **4H**$^+$			446[b]	
NH_3	−38.1	−45.1	−46.0[c]	0.9
protonated aziridine, **1A**$^+$	769.9	748.9	751.0[d]	2.1
protonated acetaldimine, **1B**$^+$	682.7	663.8	657.0[c]	−6.8
protonated azetidine, **2A**$^+$	715.6	687.4	685.6[d]	−1.8
protonated propanimine, **2B**$^+$	657.1	631.3	636.0[c]	4.7
protonated pyrrolidine, **3A**$^+$	609.4	573.8	578.0[d]	4.2
protonated butanimine, **3B**$^+$	637.2	605.0	609[e]	
protonated piperidine, **4A**$^+$			527.1[d]	
protonated pentanimine, **4B**$^+$			584[e]	

[a] From a recent reassessment[3] of the proton affinities of diamines **1**−**3**. [b] Estimated; see text. [c] From ref 11. [d] For **1A**$^+$, **2A**$^+$, **3A**$^+$, and **4A**$^+$, the corresponding $\Delta_f H°$ were calculated by combining the heats of formation[10,11] and the proton affinities[12] of aziridine, azetidine, pyrrolidine, and piperidine:

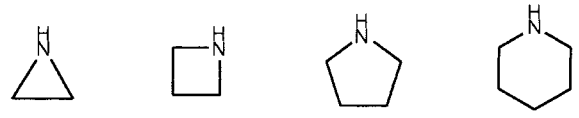

[e] Values estimated from the experimental heats of formation of **1B**$^+$ and **2B**$^+$ combined with an increment of −25 kJ/mol for the contribution of a CH_2 group.[17]

TABLE 2: CID/MIKE Spectra of $C_2H_6N^+$ Ions (*m/z* 44) [1H-NH$_3$]$^+$, 1A$^+$, and 1B$^+$ Produced by Chemical Ionization of 1,2-Ethanediamine (1) and Aziridine, and by Electron Ionization of Isopropylamine, Respectively[a]

		43	42	41	40	39	38	30	29	28	27	26	25	24	18	17	16	15	14	13	12
O_2	[**1H**-NH$_3$]$^+$	57	135	55	38	13	9	16	20	100	46	25	6	2	48	4	2	23	6	2	<1
	1B$^+$	27	78	34	21	6	3	3	62	100	41	22	4	<1	49	5	1	27	5	<1	
	1A$^+$	43	128	48	33	11	8	14	20	100	44	23	6	1	68	5	3	24	6	1	<1
N_2	[**1H**-NH$_3$]$^+$	59	106	49	36	13	9	16	11	100	52	32	10	3	39	4	5	31	16	8	4
	[**1H**-NH$_3$]$^+$*	97	97	50	36	13	9	22	11	100	49	30	9	3	31	4	5	31	15	8	3

[a] Collision gas: O_2 or N_2 as indicated in the first column.

SCHEME 2

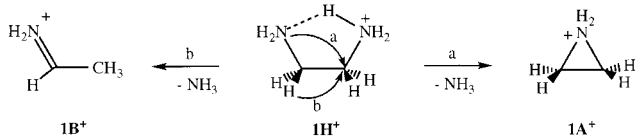

obtained, as usual, by selecting with the magnet the ion to be studied and scanning the electrostatic analyzer voltage. The kinetic energy release distribution has been derived from the analysis of the metastable peak profile using the method described in ref 6.

The collisional experiments were carried out with a VG-Analytical Auto Spec-6F mass spectrometer ($E_1B_1E_2$-$E_3B_2E_4$)[7] operating in the chemical ionization mode using methanol as reagent gas. The accelerating voltage was set at 8 kV, the electron energy at 70 eV, and the emission current at 1 mA. The source and the septum inlet temperatures were 200 and 160 °C, respectively. For the experiments using helium as target gas, the ions of interest were selected by E_1B_1 and subjected to collisional activation (CA) with helium in the third field-free region (FFR) of the instrument; the helium pressure was adjusted in order to reduce the signal to ca. 70% of its original value. The fragments were then analyzed by scanning E_2 and detected by the off-axis photomultiplier located in the fourth FFR. The CA (O_2) spectra were obtained in a similar way by selection of the ions with $E_1B_1E_2$ and collisional activation with dioxygen in a gas cell located in the fourth FFR; the fragments were

SCHEME 3

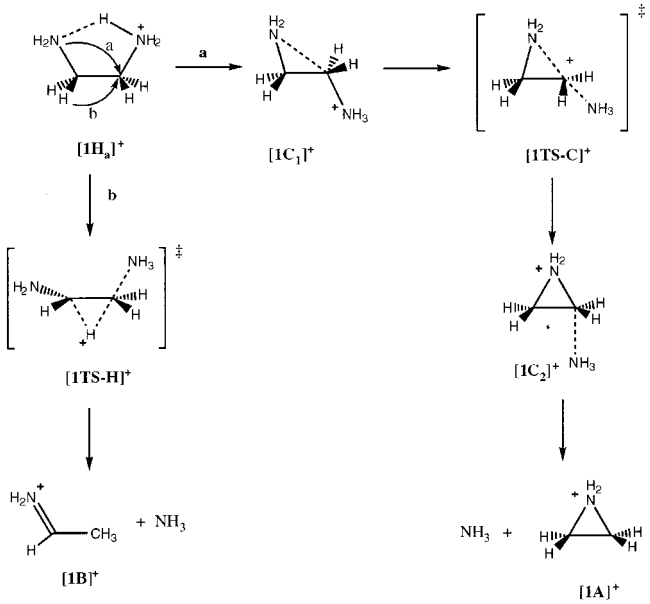

analyzed with E_3 and detected by the off-axis photomultiplier located in the fifth FFR. During the MS/MS/MS experiments, the ions produced in the third FFR by dissociation of a precursor selected by E_1B_1 were further selected by E_2 and subjected to collisional activation with O_2 in the gas cell situated before E_3; the fragments were analyzed by scanning E_3. The CA spectra

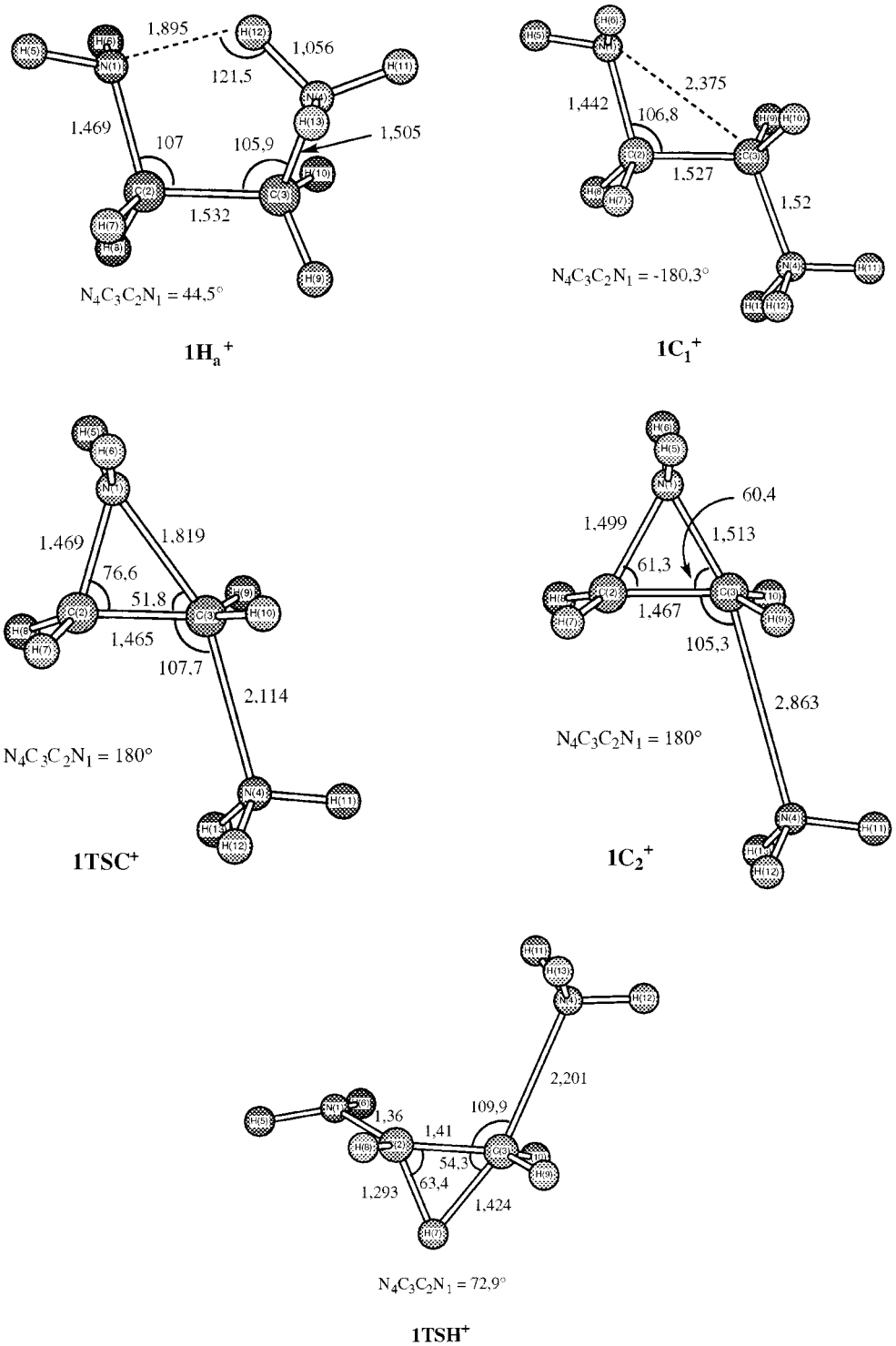

Figure 1. Optimized MP2/6-31G* geometries of the species involved during ammonia loss from protonated 1,2-ethanediamine (bond lengths in angstroms, bond angles in degrees).

presented in Tables 2, 4, 6, and 8 are the result of ≈30 signal accumulations. The chemical samples are commercial compounds (Aldrich Chemical) of research grade; high purity gases were used in the collision experiments: helium, 5.0; oxygen, 2.6; nitrogen, 5.0.

Standard ab initio molecular orbital calculations have been carried out using the Gaussian-94 series of programs.[8] The geometries of the different species investigated were first optimized at the HF/6-31G* level; the zero point energy (ZPE) has been calculated at this level after scaling by a factor 0.8929. The geometries were then refined at the MP2(FrozenCore)/6-31G* level to take electron correlation effects explicitly into account. It has been established that accurate heats of formation (i.e., ± 6 kJ·mol^{-1}) can be obtained from calculations at the G2 level of theory[9a,d] or its variants, G2(MP2)[9b,d] and G2(MP2,SVP).[9c,d] Owing to the size of the systems considered, we decided to choose the G2(MP2,SVP) technique. In this approach, the energies are calculated at the QCISD(T) level using the split-valence plus polarization (SVP) 6-31G(d) basis set. Corrections for basis set deficiencies are evaluated at the MP2/6-311+G(3df,2p) level. A higher level correction (HLC), which depends on the number of paired and unpaired electrons,

TABLE 3: Calculated Total Electronic Energies (hartrees) and Relative 0 K Energies (kJ·mol^{-1}) of the Species Relevant to the Protonated 1,2-Ethanediamine, 1H$^+$, System

	HF/6-31G*			MP2(FC)/6-31G*		G2(MP2,SVP)	
species	total	ZPE[a]	rel 0 K	total	rel 0 K	total + ZPE	rel 0 K
1H$_a^+$	−189.651 21	319	0	−190.241 58	0	−190.511 397	0
1TSR$^+$	−189.631 54	316	49	−190.217 94	60		
1C$_1^+$ (trans)	−189.636 31	316	36	−190.222 41	47		
1TSC$^+$	−189.590 84	305	144	−190.180 26	147	−190.458 389	139
1C$_2^+$	−189.609 01	306	98	−190.194 77	110		
1A$^+$	−133.407 95	214		−133.821 37		−134.003 251 1	
NH_3	−56.184 36	87		−56.354 21		−56.456 657	
1A$^+$ + NH_3	−189.592 31	301	137	−190.175 58	155	−190.459 908 1	132
1TSH$^+$	−189.564 86	295	203	−190.152 71	208	−190.442 30	181
1B$^+$	−133.442 90	207		−133.848 98		−134.034 829 4	
1B$^+$ + NH_3	−189.627 26	294	38	−190.203 19	77	−190.491 486 4	45

[a] Zero point vibrational energy (HF/6-31G(d) corrected by a factor 0.893) in kJ·mol^{-1}.

TABLE 4: CA/MIKE Spectra of $C_3H_8N^+$ Ions (*m/z* 58) [2H-NH$_3$]$^+$, 2A$^+$, and 2B$^+$ Produced by Chemical Ionization of 1,3-Propanediamine (2) and Azetidine, and by Electron Ionization of 2-Butylamine, Respectively[a]

		57	56	55	54	52	51	44	43	42	41	40	39	38	37	30	29	28	27	2 6	25	24	18
He	[**2H**-NH$_3$]$^+$	21	18	<1	1	<1			12	15	52	10	23	10	5	92	3 1	100	49	26			3
	2B$^+$	5	17	<1	3	2		3	34	50	267	15	39	13	7	52	22	100	48	22	2		5
	2A$^+$	20	16	1	2	1	<1	<1	14	16	59	9	22	10	5	96	30	100	49	27			3
O_2	[**2H**-NH$_3$]$^+$	34	69	8	15	5	2	1	13	17	49	12	24	12	7	91	39	100	41	29	8	2	1
	2B$^+$	8	58	10	15	7	2	2	27	40	131	16	33	14	8	43	43	100	37	21	5	6	2
	2A$^+$	29	70	5	12	4	1	<1	9	11	55	8	19	9	5	96	36	100	39	23	6	1	<1
N_2	[**2H**-NH$_3$]$^+$	37	51	6	11	4	1		9	13	44	10	22	11	6	82	38	100	47	33			1
	[**2H**-NH$_3$]$^+$*	48	68	5	11	5	2	2	7	9	30	8	18	10	5	77	31	100	45	29			1
	2B$^+$	9	52	2	11	5	1		26	35	124	12	31	11	5	36	24	100	43	23	5		1
	2A$^+$	37	62	4	10	3	<1		7	9	38	7	18	9	4	83	32	100	46	29	8	1	<1

[a] Collision gas: He, O_2, or N_2 as indicated in the first column.

is finally introduced. The total energy *E*[G2(MP2,SVP)] is given by

$$E[\text{G2(MP2,SVP)}] = E[\text{QCISD(T)/6-31G(d)}] + E[\text{MP2/6-311+G(3df,2p)}] - E[\text{MP2/6-31G(d)}] + \text{HLC} + \text{ZPE}$$

The HLC correction is calculated from $\text{HLC} = -An_\beta - Bn_\alpha$, with n_β and n_α being the number of β and α valence electrons, respectively ($n_\beta < n_\alpha$), and the parameters *A* and *B* are equal to 5.13×10^{-3} and 0.19×10^{-3} hartree, respectively.[9c]

Heats of formation have been evaluated from the G2(MP2,SVP) total energies by considering the atomization reactions.[9e] Using this approach, the heat of formation at 0K for a given species X, $\Delta_f H^\circ_0(\text{X})$, is given by

$$\Delta_f H^\circ_0(\text{X}) = \sum \Delta_f H^\circ_0(\text{atoms}) - \sum E[\text{G2(MP2,SVP)}](\text{atoms}) + E[\text{G2(MP2,SVP)}](\text{X}) \quad (1)$$

with *E*[G2(MP2,SVP)] = −0.5, −37.782 33, and −54.517 06 for the H, N, and C atoms, respectively. The heat of formation at 298 K is therefore given by

$$\Delta_f H^\circ_{298}(\text{X}) = \Delta_f H^\circ_0(\text{X}) + \Delta_{298} H^\circ(\text{X}) - \sum \Delta_{298} H^\circ(\text{elements}) \quad (2)$$

where the difference between the enthalpy at 298 K and that at 0 K is represented by the term $\Delta_{298}H^\circ$ ($\Delta_{298}H^\circ = H^\circ_{298} - H^\circ_0$). For the elements, experimental $\Delta_{298}H^\circ$ values have been used (i.e., 8.468, 1.050, and 8.669 kJ·mol^{-1} for $H_{2(g)}$, $C_{(s)}$, and $N_{2(g)}$, respectively), whereas for the other species the translational and rotational contributions were taken equal to 3*RT* and the vibrational contribution was estimated from the scaled (by a factor 0.893) HF/6-31G(d) vibrational frequencies.

3. Results and Discussion

Before discussing in detail each individual case, a summary of the relevant theoretical and experimental thermochemistry of the protonated α,ω-alkanediamines and their potential dissociation products is given in Table 1.

The data reported in Table 1 are indicative of the accuracy we can expect from G2(MP2,SVP) calculations on these particular systems. All the theoretical heats of formation are calculated by the atomization method described in the computational section, at the G2(MP2,SVP) level. The experimental heats of formation of protonated aziridine, azetidine, pyrrolidine, and piperidine are obtained by combining the experimental $\Delta_f H^\circ$ of the neutrals[10,11] and the proton affinity values taken from the recent compilation by Hunter and Lias.[12] The heats of formation of protonated acetaldimine and protonated propanimine are deduced from the appearance energy measurements of the corresponding ions using energy-selected electrons.[11] From examination of Table 1 it appears that the agreement between experiments and G2(MP2,SVP) computations is satisfactory since the absolute deviation is less than 7 kJ·mol^{-1}.

The second observation concerns the heats of formation of the protonated molecules. The G2(MP2,SVP) values present a decrease of 49 and 39 kJ·mol^{-1} when going from **1H$^+$** to **2H$^+$** and **3H$^+$**. Part of these differences is obviously due to the presence of an additional CH_2 group for which an enthalpy increment of −25 kJ·mol^{-1} is expected. The fact that the enthalpy difference of −39 kJ·mol^{-1} calculated between **2H$^+$** and **3H$^+$** is close to −25 kJ·mol^{-1} may be taken as evidence that, in **3H$^+$**, the strain induces only limited destabilization. Moreover, it is expected that the effect will be weakened again when passing to the species **4H$^+$**. We can thus propose that the heat of formation of the latter is situated between 439 and 453 kJ·mol^{-1}; the mean value of 446 (with a probable error of ca. 10 kJ·mol^{-1}) is indicated in Table 1.

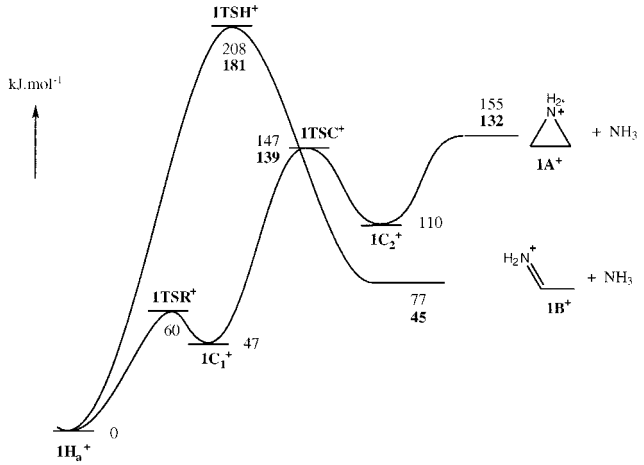

Figure 2. Calculated 0 K energy profiles for the two possible eliminations of ammonia from protonated 1,2-ethanediamine. Relative energies calculated at the MP2/6-31G*//MP2/6-31G* + ZPE level and, in bold, by the G2(MP2,SVP) method.

SCHEME 4

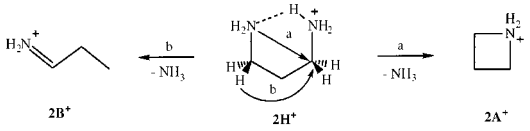

3.1. Protonated 1,2-Diaminoethane, 1H$^+$. The MIKE spectrum of protonated ethanediamine, **1H**$^+$, exhibits a major peak at *m*/*z* 44, corresponding to [**1H**-NH_3]$^+$ ions. When $\mathbf{1_{d4}D}^+$ (ND_2-$CH_2CH_2ND_2 + D^+$) ions, produced by H/D exchanges with D_2O in the inlet system, are selected, the main signal in the MIKE spectrum corresponds to [$\mathbf{1_{d4}D}$-ND_3]$^+$. The loss of ammonia consequently involves only the hydrogen atoms located initially on the nitrogen atoms; no exchange with the carbon hydrogens is observed. The metastable peak associated with the dissociation **1H**$^+ \rightarrow$ [**1H**-NH_3]$^+$ is simple Gaussian and its analysis[6] leads to the following kinetic energy releases: $T_{0.5} = 26 \pm 3$ meV and $T_{average} = 68 \pm 7$ meV.

Considering the two possible reaction mechanisms presented in Scheme 1, the deamination of **1H**$^+$ is expected to give either protonated aziridine, **1A**$^+$ (path a, Scheme 2) or protonated acetaldimine, **1B**$^+$ (path b, Scheme 2).

Structures **1A**$^+$ and **1B**$^+$ are the two most stable $C_2H_6N^+$ ions containing the CCN connectivity.[13] Experimental characterization of $C_2H_6N^+$ ions by collisional activation (CA) was presented in the literature some years ago.[14] Very similar CA spectra have been observed for ions **1A**$^+$ and **1B**$^+$ when helium is used as target gas.[14a,d] Van de Sande et al.[14d] pointed out that the peak at *m*/*z* 30 (methylene loss) is more abundant in the CA spectrum of protonated aziridine **1A**$^+$ and thus may be used as a diagnostic signal. Results obtained with the six-sector mass spectrometer of Mons University using O_2 (or N_2) as target gas are presented in Table 2. The reference ions **1A**$^+$ and **1B**$^+$ were obtained by chemical ionization of aziridine and electron ionization of isopropylamine, respectively. It is clear that the use of O_2 rather than He induces more differences in the CA mass spectra of the reference ions. Besides the two peaks at *m*/*z* 18 and 42, which are also observed in the metastable dissociations of both precursors, the major signal appears at *m*/*z* 28. It is noteworthy that an important peak at *m*/*z* 29 corresponding to a methyl loss is essentially observed for ions **1B**$^+$. Similar enhancement of the methyl loss by collision with O_2 has been observed for CH_3CHX^+ ions with X = OH, SH, or CH_3.[15] Finally, one may note that the *m*/*z* 42 signal is more intense for ions **1A**$^+$ than for ions **1B**$^+$.

SCHEME 5

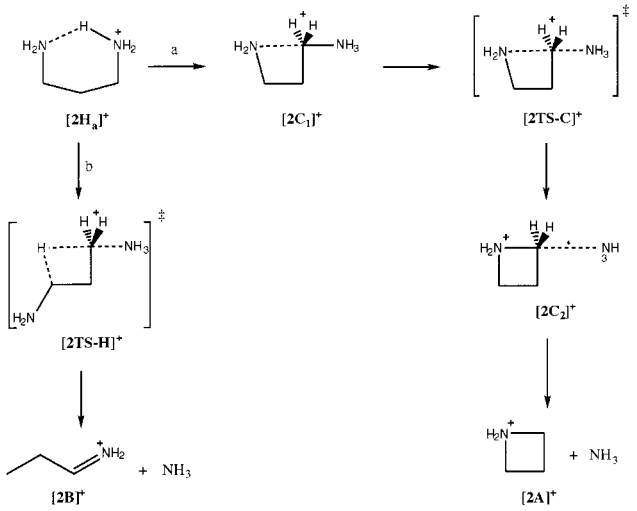

Turning now to the CA mass spectrum of ions [**1H**-NH_3]$^+$, the data quoted in Table 2 show a close similarity to that of protonated aziridine **1A**$^+$. In particular, the intensities of peaks *m*/*z* 28 and 42 are identical from one spectrum to the other. The low intensity of *m*/*z* 29 (20%) indicates the absence of [**1H**-NH_3]$^+$ ions of structure **1B**$^+$. The last collisional experiment done on this system was designed to characterize the [**1H**-NH_3]$^+$ ions originating from metastable ions **1H**$^+$ (see the experimental section for more details). The CA mass spectra of the ions [**1H**-NH_3]$^+$ produced by dissociation of **1H**$^+$ in the ion source or in flight between two sectors are given in Table 2 (N_2 was used as collision gas). Owing to the lower precision associated with the CA mass spectrum of the [**1H**-NH_3]$^+$ ions produced from metastable ions **1H**$^+$(denoted [**1H**-NH_3]$^+$* in Table 2), it can be considered that both spectra are identical.

In summary, collisional experiments demonstrate that ions **1H**$^+$, of low or high internal energy, lead to protonated aziridine, **1A**$^+$, by loss of ammonia. Considering the heats of formation of the two ions **1A**$^+$ and **1B**$^+$, this means that the dissociation of **1H**$^+$ leads to the thermochemically less favored product. This suggests that an important energy barrier prevents the formation of the most stable product **1B**$^+$. This hypothesis has been controlled by examining the two reactions with the help of ab initio molecular orbital calculations.

During the reaction modeling at the MP2/6-31G* level, it has been found that the formation of protonated aziridine, **1A**$^+$, involves three successive steps while **1B**$^+$ is produced via a 1,2-hydrogen migration together with the CN bond elongation. The various steps of these two reaction routes are summarized in Scheme 3 and the corresponding MP2/6-31G* optimized structures are presented in Figure 1. The corresponding energies are reported in Table 3 and are illustrated by the 0 K energy diagram sketched in Figure 2.

The most stable form of protonated ethanediamine, $\mathbf{1H_a}^+$ (Figure 1), is characterized by a small NCCN dihedral angle of 44.5° owing to the existence of an internal hydrogen bond.[3] The intramolecular nucleophilic substitution (reaction a, Schemes 2 and 3) needs the rear attack by the nitrogen N_1 toward the carbon C_3, i.e., the passage through a conformation developing a NCCN dihedral angle of ≈180°. The corresponding structure $\mathbf{1C_1}^+$ (Figure 1) has been found to be a minimum on the potential energy surface. It lies 47 kJ·mol^{-1} above $\mathbf{1H_a}^+$ and the rotation $\mathbf{1H_a}^+ \rightarrow \mathbf{1C_1}^+$ (**1TSR**$^+$, NCCN dihedral angle =

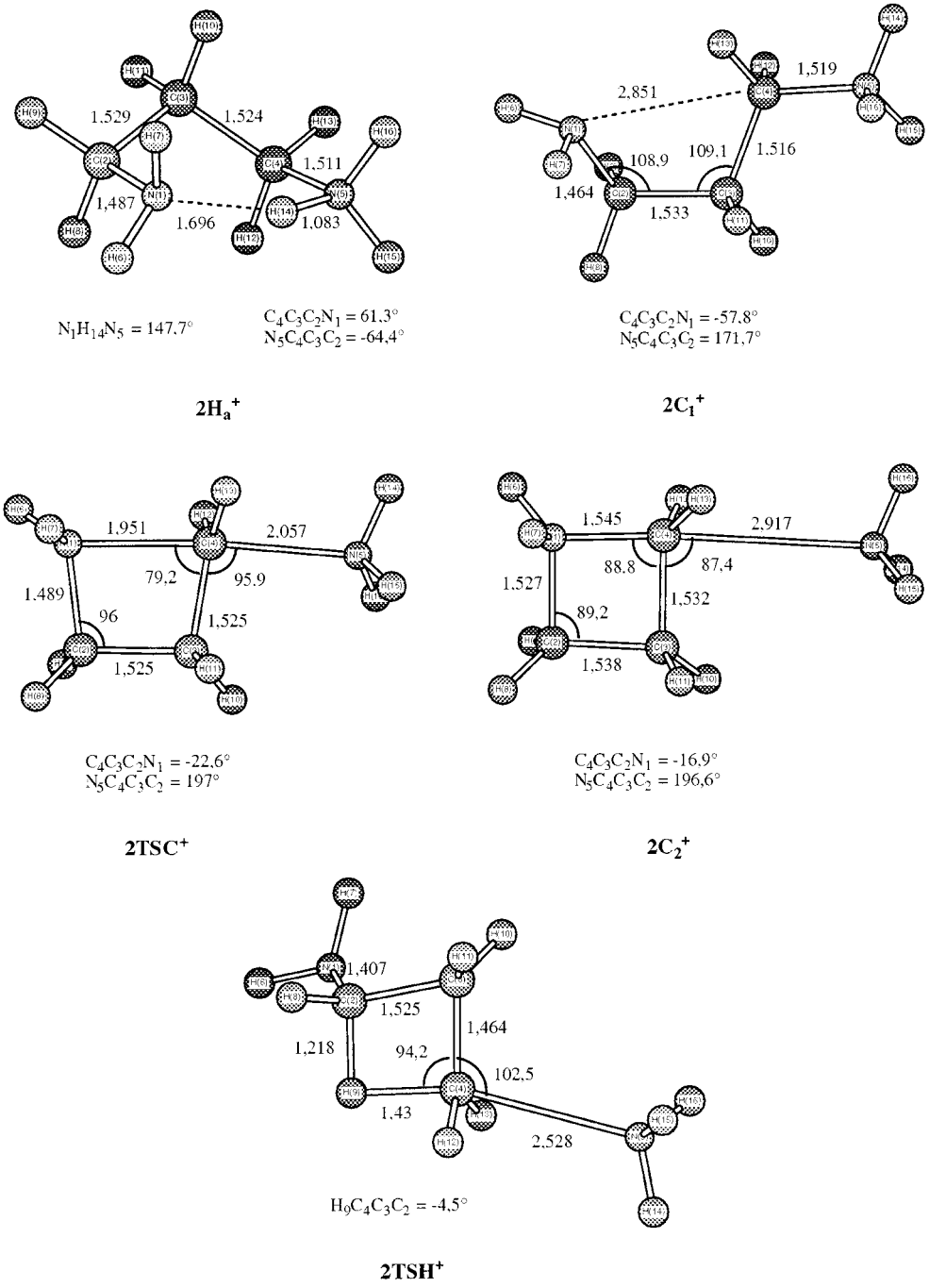

Figure 3. Optimized MP2/6-31G* geometries of the species involved during ammonia loss from protonated 1,3-propanediamine (bond lengths in angstroms, bond angles in degrees).

128°) involves a barrier of 60 kJ·mol^{-1} (Table 3, Figure 2). The shortening of the N_1–C_3 distance is accompanied by an increase of the potential energy until attainment of a maximum, 147 kJ·mol^{-1} above **1H$_a^+$**, for the transition structure **1TSC**$^+$ (Figure 1), which connects **1C$_1^+$** and **1C$_2^+$**. The latter structure is clearly a complex between protonated aziridine and the molecule of ammonia, and it is characterized by a C−NH_3 distance of 2.86 Å (Figure 1). This complex is 110 kJ·mol^{-1} above **1H$_a^+$** and only 45 kJ·mol^{-1} below its components (Table 3, Figure 2). The C−NH_3 lengthening leads to the separated products, protonated aziridine **1A**$^+$ + NH_3, by a continuously endothermic process. At the MP2/6-31G*+ZPE level of theory, it is difficult to decide which is the energy determining step of the overall reaction a. The formation of the complex **1C$_2^+$** via the transition structure **1TSC**$^+$ and its dissociation into **1A**$^+$ + NH_3 through a loose transition state are calculated to be too close together (147 and 155 kJ·mol^{-1}, respectively). This ambiguity is not resolved at the higher G2(MP2,SVP) level, since **1TSC**$^+$ is calculated to be 7 kJ·mol^{-1} above **1A**$^+$ + NH_3.

The second reaction (path b, Schemes 2 and 3) involves a 1,2-hydride ion migration together with the separation of the molecule of ammonia. The transition structure of this reaction, **1TSH**$^+$ (Figure 1) is situated 208 kJ·mol^{-1} above **1H$_a^+$** at the MP2/6-31G*+ZPE level and 181 kJ·mol^{-1} above **1H$_a^+$** at the G2(MP2,SVP) level (Table 3). What is clearly evident from the examination of Figure 2 is that **1TSH**$^+$ is well above the energy determining step of reaction a (**1TSC**$^+$ or **1A**$^+$ + NH_3): the energy difference is 61−42 kJ·mol^{-1} depending upon the level of theory used in the calculations. This large energy difference explains why the **1H**$^+$ ions prefer to dissociate via

TABLE 5: Calculated Total Electronic Energies (hartrees) and Relative 0 K Energies (kJ·mol^{-1}) of the Species Relevant to the Protonated 1,3-Propanediamine, 2H$^+$, System

	HF/6-31G*			MP2(FC)/6-31G*		G2(MP2,SVP)	
species	total	ZPE[a]	rel 0 K	total	rel 0 K	total + ZPE	rel 0 K
2H$_a$ $^+$	−228.694 88	392	0	−229.418 92	0	−229.745 173	0
2H$_b$ $^+$	−228.672 75	389	55	−229.389 84	73		
2C$_1$ $^+$	−228.678 91	390	40	−229.397 14	55		
2TSC$^+$	−228.631 72	380	154	−229.352 32	163	−229.686 89	153
2C$_2$ $^+$	−228.659 57	381	82	−229.376 32	101		
2A$^+$	−172.459 86	289		−173.003 78		−173.241 850 3	
NH_3	−56.184 36	87		−56.354 21		−56.456 657	
2A$^+$ + NH_3	−228.644 22	376	117	−229.357 99	144	−229.698 507 3	120
2TSH$^+$	−228.586 97	366	257	−229.307 05	268	−229.655 1	236
2B$^+$	−172.481 22	280		−173.018 45		−173.264 134 6	
2B$^+$ + NH_3	−228.665 58	367	52	−229.372 66	96	−229.720 791 6	61

[a] Zero point vibrational energy (HF/6-31G(d) corrected by a factor 0.893) in kJ·mol^{-1}.

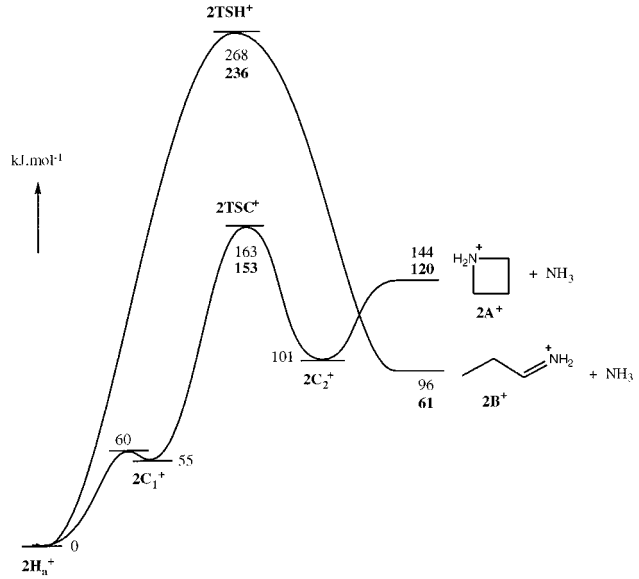

Figure 4. Calculated 0 K energy profiles for the two possible eliminations of ammonia from protonated 1,3-propanediamine. Relative energies calculated at the MP2/6-31G*//MP2/6-31G* + ZPE level and, in bold, by the G2(MP2,SVP) method.

SCHEME 6

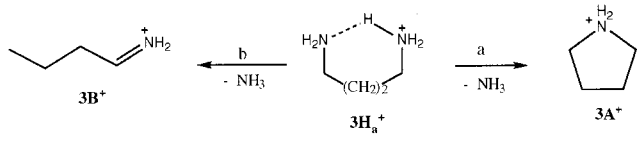

the internal nucleophilic substitution reaction a rather than reaction b even though the latter leads to the more stable products **1B**$^+$ + NH_3.

3.2. Protonated 1,3-Propanediamine, 2H$^+$. Unimolecular decomposition of metastable ions **2H**$^+$ leads exclusively to [**2H**-NH_3]$^+$ ions. The corresponding peak observed in the MIKE spectrum is simple Gaussian and is characterized by kinetic energy release values of $T_{0.5} = 35 \pm 4$ meV and $T_{average} = 98 \pm 10$ meV. As already observed with 1,2-ethanediamine, **1**, H/D exchange with D_2O in the ion source demonstrates that the ammonia loss from **2H**$^+$ involves exclusively the N-bonded hydrogen atoms.

The two possible products of the loss of ammonia from **2H**$^+$ are protonated azetidine, **2A**$^+$ (path a, Scheme 4) and protonated propanimine, **2B**$^+$ (path b, Scheme 4).

The latter ion is the most stable structure in the $C_3H_8N^+$ series: protonated azetidine **2A**$^+$ is less stable by 56 kJ·mol^{-1} (Table 1). The CA mass spectra of several $C_3H_8N^+$ ions have been presented in the literature,[14b,e] but none of these studies reported the spectrum of protonated azetidine. The results obtained using the six-sector mass spectrometer for the two reference ions **2A**$^+$ and **2B**$^+$ and for the [**2H**-NH_3]$^+$ fragment ions are presented in Table 4.

Whatever the target gas used during the collisional experiments (He, O_2, or N_2), the two ion structures **2A**$^+$ and **2B**$^+$ can be identified using the *m*/*z* 57, 39−43, 30, and 28 peak intensities. The two main pieces of diagnostic information are (i) the peak at *m*/*z* 41 is the base peak of the CA mass spectrum of protonated propanimine **2B**$^+$ and (ii) the signals at *m*/*z* 57 and 30 are larger in the CA mass spectrum of protonated azetidine **2A**$^+$. Comparison with the CA mass spectra of [**2H**-NH_3]$^+$ ions reveals that the latter are essentially protonated azetidine **2A**$^+$. This conclusion is also valid for the [**2H**-NH_3]$^+$ ions coming from dissociation of metastable **2H**$^+$ ions (noted [**2H**-NH_3]$^+$* in Table 4, target gas = N_2). Thus, protonated 1,3-propanediamine ions **2H**$^+$ of low or high internal energy lead to the cyclized deamination product. As noted above in the case of protonated 1,2-ethanediamine **1H**$^+$, the loss of ammonia conducts to the least stable products. This suggests again the existence of a large energy barrier for the process leading to the most stable products **2B**$^+$ + NH_3. This point is confirmed by ab initio molecular orbital calculations.

The detailed mechanism of the two reaction routes is presented in Scheme 5.

The MP2/6-31G* exploration of the internal nucleophilic substitution (path a) reveals again that the reaction proceeds in two steps involving the passage through two stable intermediates **2C$_1$**$^+$ and **2C$_2$**$^+$. The hydride ion migration (path b) is coupled with the CN bond elongation and occurs in one step. The corresponding structures and energies are presented in Figure 3 and Table 5, respectively.

The most stable form of protonated 1,3-propanediamine, structure **2H$_a$**$^+$ (Figure 3), presents clearly an internal hydrogen bond.[3,16] This conformation is more stable than the "zigzag" conformation, **2H$_b$**$^+$, where the NCCCN frame is fully extended, by 73 kJ·mol^{-1} (MP2/6-31G*, Table 5). The internal nucleophilic substitution needs first the conformational change **2H$_a$**$^+$ → **2C$_1$**$^+$ in order to prepare the rear attack by the NH_2 group toward the nucleophilic center. This rearrangement is accompanied by the breaking of the internal hydrogen bond and thus requires an appreciable amount of energy. Accordingly, the critical point is situated 60 kJ·mol^{-1} above **2H$_a$**$^+$. The intermediate ion **2C$_1$**$^+$ (relative MP2/6-31G* energy 55 kJ·mol^{-1}, Table 5) finds its stability in a small favorable interaction

TABLE 6: CA/MIKE Spectra of $C_4H_{10}N^+$ Ions (*m/z* 72) $[3H\text{-}NH_3]^+$, $3A^+$, and $3B^+$ Produced by Chemical Ionization of 1,4-Butanediamine (3) and Pyrrolidine, and by Electron Ionization of 2-Pentylamine, Respectively[a]

		71	70	69	68	67	57	56	55	54	53	52	51	50	44
He	$[\mathbf{3H}\text{-}NH_3]^+$	9	11	4	6	<1	<1	2	19	5	6	3	4	3	15
	$\mathbf{3B}^+$	1	3	1	1		6	52	58	14	9	7	7	6	30
	$\mathbf{3A}^+$	21	10	3	5	<1	<1	2	11	4	5	2	3	2	12
O_2	$[\mathbf{3H}\text{-}NH_3]^+$	10	20	7	18	2	2	3	15	5	5	3	3	3	9
	$\mathbf{3B}^+$	2	7	2	2	1	<1	78	37	18	7	7	6	4	19
	$\mathbf{3A}^+$	30	21	5	15	<1	<1	1	6	2	2	<1	1	1	4
N_2	$[\mathbf{3H}\text{-}NH_3]^+$	15	23	7	17	<1		<1	11	3	3	1	2	1	6
	$[\mathbf{3H}\text{-}NH_3]^+$*	11	25	9	18	2		2	9	5	5	3	3	3	7
	$\mathbf{3B}^+$	6	10	4	2		3	67	38	17	6	6	5	4	18
	$\mathbf{3A}^+$	42	29	6	18	<1		<1	6	2	2	<1	1	1	4

		43	42	41	40	39	38	37	30	29	28	27	26	18	15
He	$[\mathbf{3H}\text{-}NH_3]^+$	100	48	54	17	46	12	5	267	23	91	54	18	<1	2
	$\mathbf{3B}^+$	100	78	61	17	54	14	6	383	62	139	103	22		
	$\mathbf{3A}^+$	100	47	53	15	43	11	4	205	19	84	47	15		
O_2	$[\mathbf{3H}\text{-}NH_3]^+$	100	36	44	14	33	12	7	158	11	48	22	11	<1	<1
	$\mathbf{3B}^+$	100	61	52	19	43	17	10	131	41	88	49	19	1	1
	$\mathbf{3A}^+$	100	40	53	17	30	10	4	133	8	48	20	8		
N_2	$[\mathbf{3H}\text{-}NH_3]^+$	100	43	54	17	45	7	3	176	18	86	53	29	1	1
	$[\mathbf{3H}\text{-}NH_3]^+$*	100	40	50	18	42	6	3	149	17	81	49	28	3	3
	$\mathbf{3B}^+$	100	72	58	23	53	22	10	176	46	128	90	35	2	4
	$\mathbf{3A}^+$	100	40	53	17	43	18	9	147	18	90	53	30	<1	1

[a] Collision gas: He, O_2, or N_2 as indicated in the first column.

SCHEME 7

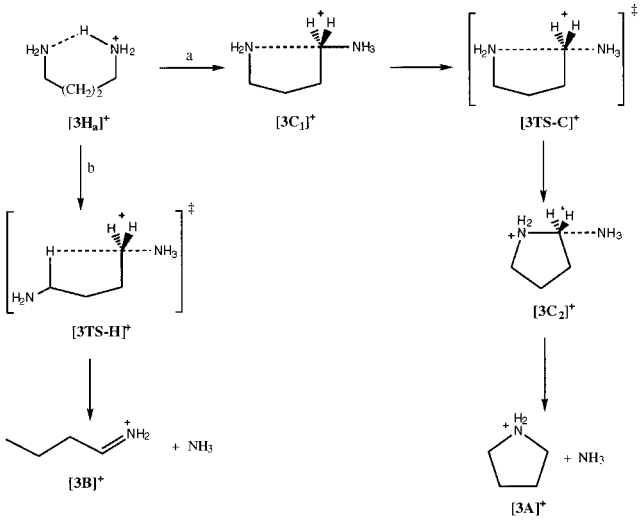

between the nucleophilic NH_2 group and the electron-deficient carbon C_4. When the distance between these two reactive centers is shortened, the NH_3 molecule begins to move away and the energy increases markedly until attainment of the transition structure $\mathbf{2TSC}^+$ situated 163 kJ·mol^{-1} above $\mathbf{2H_a}^+$. This point corresponds to the energy determining step of the overall reaction a (Scheme 5) as illustrated by the energy profile presented in Figure 4.

In fact, after the passage through $\mathbf{2TSC}^+$, the structure $\mathbf{2C_2}^+$, which is a complex between protonated azetidine and the NH_3 molecule, is produced. In this complex, situated 101 kJ·mol^{-1} above $\mathbf{2H_a}^+$, the C−NH_3 distance (2.92 Å, Figure 3) is far from a covalent bond length and the separation of the products $\mathbf{2A}^+ + NH_3$ needs only the endothermicity of the process, i.e., 43 kJ·mol^{-1}. The MP2/6-31G*+ZPE relative energy of $\mathbf{2TSC}^+$ with respect to $\mathbf{2A}^+ + NH_3$ is 19 kJ·mol^{-1}, a difference which is close to the expected precision of the calculations at this level. It is noteworthy, however, that this energy difference is conserved at the higher G2(MP2,SVP) level (33 kJ·mol^{-1}, Table 5). The fact that $\mathbf{2TSC}^+$ constitutes the highest point in the energy surface of the internal nucleophilic substitution reaction a seems consequently confirmed.

The second possible reaction (b, Scheme 5) is the 1,3-hydride ion migration. We found that this reaction requires considerable critical energy. The characterized transition structure $\mathbf{2TSH}^+$, localized at the MP2/6-31G* level, is situated 268 kJ·mol^{-1} above $\mathbf{2H_a}^+$. At the G2(MP2,SVP) level this energy difference reduces to 236 kJ·mol^{-1}. It is, however, evident that $\mathbf{2TSH}^+$ is higher than $\mathbf{2TSC}^+$, by no less than 83 kJ·mol^{-1} at the G2-(MP2,SVP) level. Consequently, the calculations confirm nicely the expectation, based on the experimental observation, that a large energy barrier prevents the formation of the most stable deamination products thus allowing the system to evolve via the internal nucleophilic substitution reaction.

3.3. Protonated 1,4-Butanediamine, $\mathbf{3H}^+$. The MIKE spectrum of protonated 1,4-butanediamine, $\mathbf{3H}^+$, presents only one peak of Gaussian shape at *m/z* 72. Analysis of the peak profile leads to the estimate of the kinetic energy release values: $T_{0.5} = 54 \pm 5$ meV and $T_{average} = 162 \pm 16$ meV. The molecule of ammonia eliminated from $\mathbf{3H}^+$ contains exclusively hydrogen originating from the nitrogen atoms as demonstrated by H/D exchange experiments.

The two $C_4H_{10}N^+$ ions expected to be produced by the internal nuclophilic substitution and by the hydride ion migration are protonated pyrrolidine, $\mathbf{3A}^+$, and protonated butaneimine, $\mathbf{3B}^+$, respectively (Scheme 6). These two ions can be, a priori, purely formed by protonation of pyrrolidine and by electron ionization of 2-aminopentane and characterized by their collisional activation spectra. The CA mass spectra of these $C_4H_{10}N^+$ reference ions and of the $[\mathbf{3H}\text{-}NH_3]^+$ ions produced either in the source or in a field-free region of the six-sector instrument are reported in Table 6. The O_2 CA spectrum of protonated pyrrolidine, $\mathbf{3A}^+$, agree perfectly with the recently published data of Frosing and Turecek.[18]

Several characteristic features are observed between the CA spectra of $\mathbf{3A}^+$ and $\mathbf{3B}^+$, particularly in the regions *m/z* 27−29, 42−44, 54−56, and 70−71. For example, the presence of an intense signal at *m/z* 56 is characteristic of structure $\mathbf{3B}^+$ while peaks at *m/z* 71 and 70 are specific for structure $\mathbf{3A}^+$.

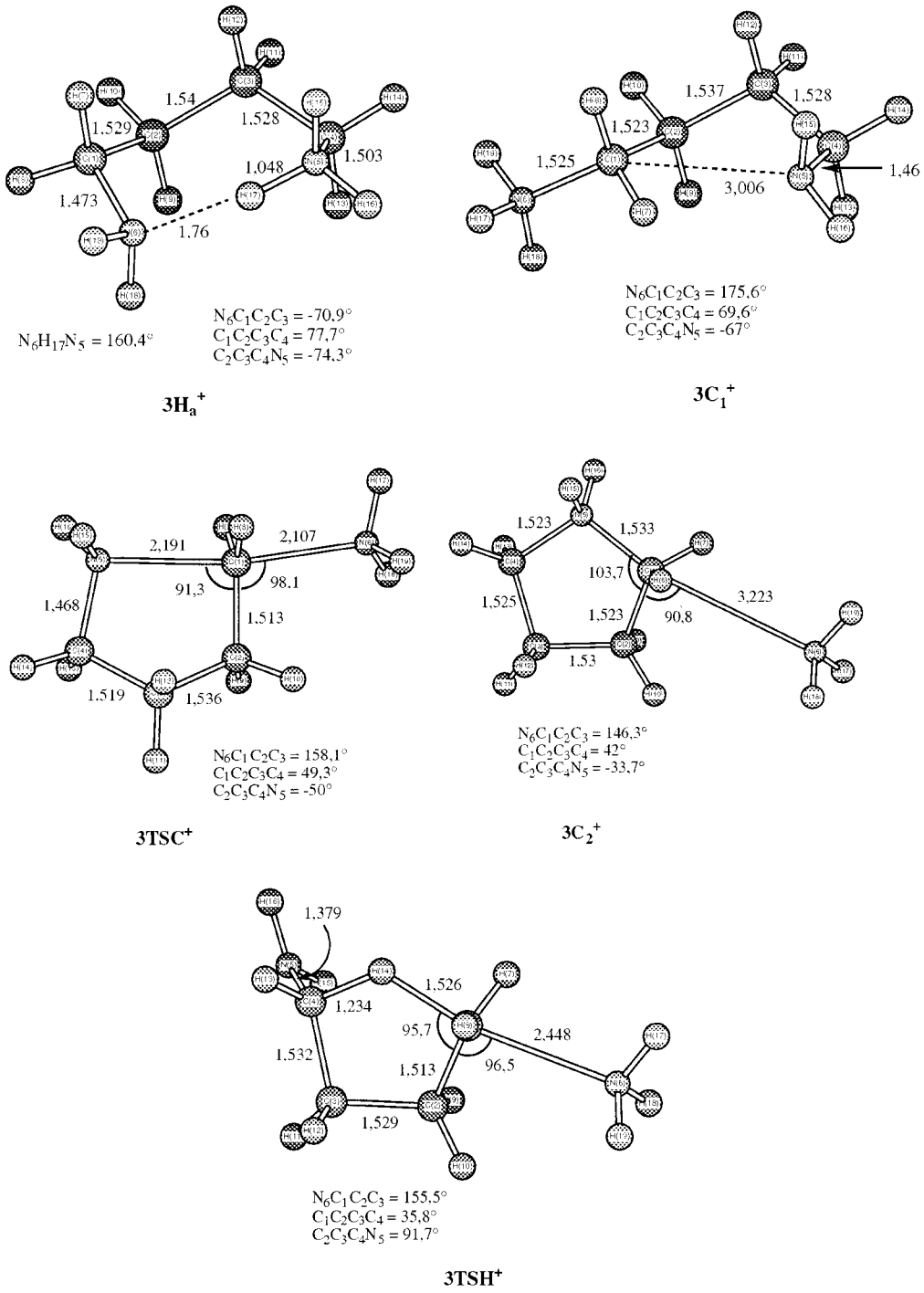

Figure 5. Optimized HF/6-31G* geometries of the species involved during ammonia loss from protonated 1,4-butanediamine (bond lengths in angstroms, bond angles in degrees).

Considering the CA spectra of [**3H**-NH_3]$^+$ ions, they present significant peaks at *m*/*z* 71 and 70 and a negligible signal at *m*/*z* 56. These observations indicate that the $C_4H_{10}N^+$ ions coming from **3H**$^+$ are essentially protonated pyrrolidine **3A**$^+$. This conclusion stands for the [**3H**-NH_3]$^+$ ions produced in the ion source as well as in the field-free region.

The various reaction intermediates involved during reactions a and b from protonated 1,4-butanediamine **3H**$^+$ are summarized in Scheme 7. Considering the size of the system, the complete investigation of the corresponding part of the potential energy surface has been done at the simple HF/6-31G* level. The energies have been then evaluated at the MP2/6-31G*//HF/6-31G*+ZPE level. More elaborate G2(MP2,SVP) calculations have been undertaken for the transition structures associated with the energy determining steps of each reaction route. These data were used to construct the energy diagram presented in Figure 6. The optimized structures and the calculated total and relative energies are presented in Figure 5 and Table 7, respectively.

The most stable structure of protonated 1,4-butanediamine is the pseudo chair structure $\mathbf{3H_a}^+$ (Figure 5). As expected, the internal hydrogen bond is shorter in $\mathbf{3H_a}^+$ than in the lower homologues (1.76 Å for $\mathbf{3H_a}^+$ but 1.882 Å for $\mathbf{2H_a}^+$, HF/6-31G* optimized geometries). In the same vein, the N−H···N bond angle is larger for $\mathbf{3H_a}^+$ (≈160° compared to ≈148° for $\mathbf{2H_a}^+$). As a consequence, the stabilization energy

TABLE 7: Calculated Total Electronic Energies (hartrees) and Relative 0 K Energies (kJ·mol^{-1}) of the Species Relevant to the Protonated 1,4-Propanediamine, 3H$^+$, System

	HF/6-31G*			MP2/6-31G* [b]		G2(MP2,SVP)	
species	total	ZPE[a]	rel 0 K	total	rel 0 K	total 0 K	rel 0 K
3H$_a$ $^+$	−267.734 31	464	0	−268.588 43	0	−268.975 175	0
3H$_b$ $^+$ (trans)	−267.708 29	460	64	−268.554 38	85		
3C$_1$ $^+$	−267.716 11	462	46	−268.564 39	61		
3TSC$^+$	−267.682 74	454	125	−268.531 83	139	−268.927 259	126
3C$_2$ $^+$	−267.727 00	456	11	−268.574 74	28		
3A$^+$	−211.528 94	365		−212.204 94		−212.500 126 5	
NH_3	−56.184 36	87		−56.353 71		−56.456 657	
3A$^+$ + NH_3	−267.713 30	452	43	−268.558 65	66	−268.956 783 5	45
3TSH$^+$	−267.621 34	438	271	−268.471 16	282	−268.884 323	238
3B$^+$	−211.517 55	352		−212.183 99		−212.489 531	
3B$^+$ + NH_3	−267.701 91	439	60	−268.537 70	108	−268.946 188	73

[a] Zero point vibrational energy (HF/6-31G(d) corrected by a factor 0.893) in kJ·mol^{-1}. [b] Single point calculations using the HF/6-31G* optimized geometries.

TABLE 8: CA/MIKE Spectra of $C_5H_{12}N^+$ Ions (*m/z* 86) [4H-NH$_3$]$^+$, 4A$^+$, and 4B$^+$ Produced by Chemical Ionization of 1,5-Pentanediamine (4) and Piperidine, and by Electron Ionization of 3-Heptylamine, Respectively[a]

		85	84	83	82	80	72	70	69	68	67	65	56	54	53
He	[**4H**-NH$_3$]$^+$	10	14	1	2	1	1	3	48	7	5	1	100	15	11
	4B$^+$	2	1		<1			4	73	2	3	1	100	13	7
	4A$^+$	37	15	1	2	<1		2	33	6	4	<1	100	14	10
O_2	[**4H**-NH$_3$]$^+$	49	28		8	3		7	72	14	10	2	100	17	11
	4B$^+$	2	3	3	3	3		5	59	5	6	2	100	14	6
	4A$^+$	70	33		8	3		6	36	11	7	<1	100	16	9
N_2	[**4H**-NH$_3$]$^+$	36	34	5	10	4		6	52	13	8	2	100	18	12
	[**4H**-NH$_3$]$^+$*	15	34	5	9	4	8	6	35	12	7	2	100	17	12
	4B$^+$	7	6	3	5	2		6	48	5	5	2	100	15	8
	4A$^+$	64	36	6	10	4		5	31	11	7	2	100	18	11
		52	51	50	44	43	42	41	39	30	29	28	27	18	15
He	[**4H**-NH$_3$]$^+$	5	5	3	19	42	44	99	60	251	41	65	44	<1	<1
	4B$^+$	4	4	2	40	102	58	89	51	196	36	60	44	<1	<1
	4A$^+$	4	4	3	14	33	36	67	43	147	26	40	23		
O_2	[**4H**-NH$_3$]$^+$	6	7	6	14	34	29	55	34	130	20	35	20	1	
	4B$^+$	5	6	5	24	82	41	53	32	86	22	40	24	1	<1
	4A$^+$	5	5	4	10	34	27	41	28	98	16	31	16		
N_2	[**4H**-NH$_3$]$^+$	8	8	8	13	33	35	63	56	166	40	81	61	3	3
	[**4H**-NH$_3$]$^+$*	7	8	7	12	32	32	54	50	144	37	74	56	2	2
	4B$^+$	7	7	6	23	81	49	63	47	88	31	69	51	1	3
	4A$^+$	7	8	7	11	31	33	52	50	140	37	75	56	2	2

[a] Collision gas: He, O_2, or N_2 as indicated in the first column.

of **3H$_a$**$^+$ is larger; an estimate of ≈85 kJ·mol^{-1} is given by the energy difference between **3H$_a$**$^+$ and the linear conformer **3H$_b$**$^+$ (Table 7).

The internal substitution reaction a is again characterized by the initial formation of an intermediate, **3C$_1$**$^+$, where a favorable interaction is allowed between the nucleophilic NH_2 group and the electron-deficient carbon atom. This structure is situated 61 kJ·mol^{-1} above **3H$_a$**$^+$, and its formation needs only 5 kJ·mol^{-1} of excess potential energy at the MP2/6-31G* level. The cyclization step **3C$_1$**$^+$ → **3C$_2$**$^+$ is energy determining for the overall reaction a. The transition structure **3TSC**$^+$ is 139 kJ·mol^{-1} (126 kJ·mol^{-1} at the G2(MP2,SVP) level) above **3H$_a$**$^+$. At this stage the carbon atom is approximately at the same distance from both nitrogen atoms and the increase of the C_1-N_6 distance is accompanied by a considerable gain in energy until attainment of the stationary point **3C$_2$**$^+$. This structure is a complex between protonated pyrrolidine **3A**$^+$ and a molecule of ammonia. It is stabilized by 38 kJ·mol^{-1} with respect to its components, and no reverse activation energy seems to be associated with the dissociation **3C$_2$**$^+$ → **3A**$^+$ + NH_3.

The second possible process, the 1,4-hydride ion transfer b (Scheme 7), involves a transition structure **3TSH**$^+$ of high energy. At the simple MP2/6-31G*//HF/6-31G*+ZPE level **3TSH**$^+$ is situated 282 kJ·mol^{-1} above **3H$_a$**$^+$; this energy difference reduces to 238 kJ·mol^{-1} at the G2(MP2,SVP) level. It is clear, however, that **3TSH**$^+$ is higher than **3TSC**$^+$ and that the former process could not compete with the latter at any energy regime. Consequently, at low or at high internal energy of the reactant **3H**$^+$, the only observed ammonia loss leads to protonated pyrrolidine **3A**$^+$. It is noteworthy that, contrary to the previously examined protonated diamines **1H**$^+$ and **2H**$^+$, the structure formed corresponds also to the more stable ionic product which may be produced by the deamination reactions.

3.4. Protonated 1,5-Pentanediamine, 4H$^+$. Finally, only experimental results concerning protonated 1,5-pentanediamine **4H**$^+$ will be reported. The size of the system as well as the obvious conclusions that may be drawn from the three lowest homologues renders unnecessary a theoretical investigation of this molecule.

The ammonia loss is the only fragmentation of **4H**$^+$ metastable ions. Deuterium labeling demonstrates that the eliminated molecule of ammonia contains exclusively hydrogen originally bonded to the nitrogen atoms of **4H**$^+$. The corresponding peak in the MIKE spectrum is simple Gaussian, and the kinetic energy release values deduced from the analysis of the peak profile are $T_{0.5} = 83 \pm 8$ meV and $T_{average} = 218 \pm 20$ meV.

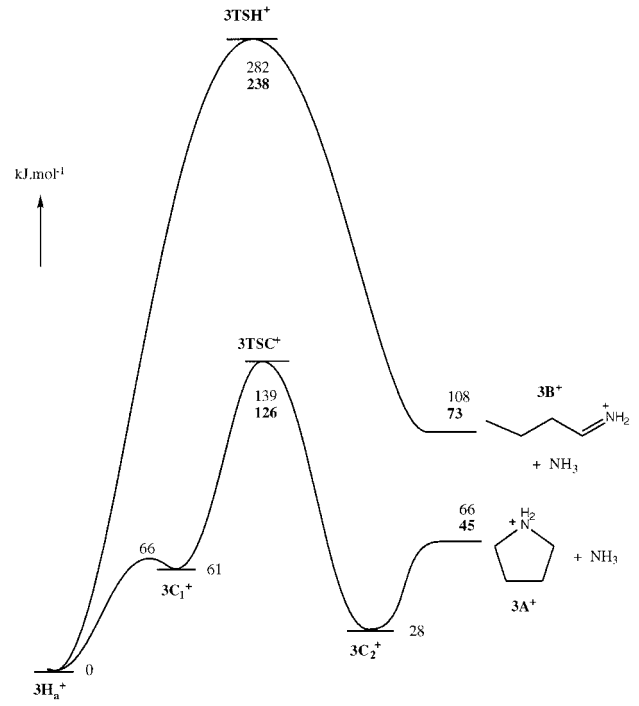

Figure 6. Calculated 0 K energy profiles for the two possible eliminations of ammonia from protonated 1,4-butanediamine. Relative energies calculated at the MP2/6-31G*//MP2/6-31G* + ZPE level and, in bold, by the G2(MP2,SVP) method.

SCHEME 8

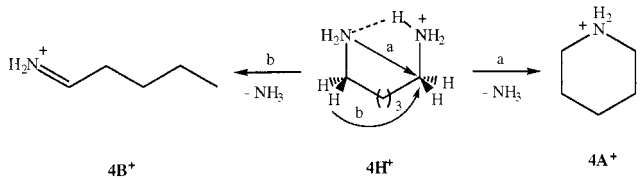

The two possible $C_5H_{12}N^+$ ions expected from reactions a and b are protonated piperidine $\mathbf{4A}^+$ or protonated pentanimine $\mathbf{4B}^+$ (Scheme 8). These two structures can be produced by chemical ionization of piperidine and electron ionization of a suitable amine, respectively, and identified by their collisional activation spectra (Table 8). As observed in Table 8, prominent differences appear in the *m*/*z* 85−84 and *m*/*z* 39−44 regions. In particular, an important peak at *m*/*z* 43 is characteristic of the protonated pentanimine structure while peaks at *m*/*z* 85 and 84 signal the presence of protonated piperidine. It is apparent that the CA spectra (obtained using He, O_2, or N_2 as target gas) of $C_5H_{12}N^+$ ions coming from protonated 1,5-pentanediamine, $\mathbf{4H}^+$, are identical with that of protonated piperidine. Moreover, the CA spectrum of the $C_5H_{12}N^+$ ions originating from dissociation of metastable ions $\mathbf{4H}^+$ (denoted $[\mathbf{4H}\text{-}NH_3]^{+}$* in Table 8) is identical with that of the $[\mathbf{4H}\text{-}NH_3]^+$ ions produced in the ion source. One may thus conclude that protonated piperidine $\mathbf{4A}^+$ is the exclusive deamination product of $\mathbf{4H}^+$ at low and at high internal energy. As observed for the three previous cases, the most favorable reaction of deamination is the internal nucleophilic substitution. Furthermore, as also observed for the 1,3-diamino derivative $\mathbf{3H}^+$, the structure formed corresponds to the most stable ion. Considering the results obtained for the three first systems, one may expect that the exclusive formation of $\mathbf{4A}^+$ is due, again, to a lower critical energy for this process.

Conclusion

The present study demonstrates that protonated α,ω-alkanediamines eliminate a molecule of ammonia exclusively via an internal nucleophilic substitution process (SN_i, reaction a) even when the product ion is not the most stable. Molecular orbital calculations indicate that the reaction proceeds via two intermediate structures ($\boldsymbol{n}\mathbf{C_1}$ and $\boldsymbol{n}\mathbf{C_2}$) separated by a significant energy barrier. This situation is reminiscent of the double-well potential energy surface associated with intermolecular SN_2 reactions involving cationic substrates.[19]

The size of the molecule appears to have a strong effect on the potential energy profile of the SN_i reaction. As the number of carbon atoms increases, the stability of the protonated cyclic amine increases. Consequently, the transition structure $\boldsymbol{n}$**TSC** is increasingly higher in energy than the fragments and the transient complex $\boldsymbol{n}\mathbf{C_2}$ contains an increasingly large amount of internal energy. This is corroborated by the observation of an increase ot the *T* value associated with the ammonia loss from metastable ions when passing from $\mathbf{1H}^+$ to $\mathbf{4H}^+$, although this increase is also partly due to a degree of freedom effect.

The second possible reaction mechanism for the ammonia loss from protonated α,ω-alkanediamines, the hydride shift b, is never observed. Molecular orbital calculations show that it is a one-step process where the hydride ion approach occurs together with the C−N bond elongation. This reaction is associated with a critical energy so large that it renders impossible its competition with reaction a. The calculated 0 K critical energy differences between processes b and a are 43, 75, and 111 kJ·mol^{-1} for $\mathbf{1H}^+$, $\mathbf{2H}^+$, and $\mathbf{3H}^+$, respectively. This increase with the size of the system is obviously due to the increase of stability of the cyclic structures $\boldsymbol{nA}^+$ with respect to $\boldsymbol{nB}^+$ when *n* increases. In this context the behavior of the fourth protonated molecule, $\mathbf{4H}^+$, is not unexpected.

It is tempting to compare the present data with the results obtained for the corresponding diols.[3] In the latter case it has been concluded that protonated 1,2-ethanediol gives exclusively reaction b (the pinacol rearrangement) while protonated 1,4-butanediol and protonated 1,5-pentanediol give only reaction a. Protonated 1,3-propanediol evolves via reaction a at low internal energy and reaction b at high internal energy. The reason for this constrasting behavior is the comparable values for the critical energies of both processes for 1,2-ethanediol and 1,3-propanediol. This means, in particular, that the critical energy for reaction b is noticeably lower in the case of the diols than of the diamines, as indicated by the calculations. This phenomenon finds its origin in the difference of dissociation energies of C−XH$^+$ (X = O, N) bonds. For example, the enthalpy variations associated with (i) $CH_3OH_2^+ \rightarrow CH_3^+ + OH_2$ and (ii) $CH_3NH_3^+ \rightarrow CH_3^+ + NH_3$ are 280 and 440 kJ·mol^{-1}, respectively, in keeping with the ability of the heteroatoms to share their lone pair electrons. Thus, the dissociation of a C−N bond requires more energy than a C−O bond in the protonated species. This is exactly what is reflected by the high critical energies for reaction b in the case of N with respect to O. The phenomenon is less pronounced, if existing, for the SN_i reaction since the C−X bond breaking is (partly) compensated by a C−X bond forming.

References and Notes

(1) See, for example: Lee, S. J.; Mhin, B. J.; Cho, S. J.; Lee, J. Y.; Kim, K. S. *J. Phys. Chem.* **1994**, *98*, 1129.

(2) (a) Aue, D. H.; Webb, H. M.; Bowers, M. T. *J. Am. Chem. Soc.* **1973**, *95*, 2699. (b) Bowers, M. T. *Gas Phase Ion Chemistry*; Academic

Press: New York, 1979; Vol. 2. (c) Yamdagni, R.; Kebarle, P. *J. Am. Chem. Soc.* **1973**, *95*, 3504. (d) Meot-Ner (Mautner), M.; Hamlet, P.; Hunter, E. P.; Field, F. H. *J. Am. Chem. Soc.* **1980**, *102*, 6393.

(3) Bouchoux, G.; Choret, N.; Berruyer-Penaud, F. *J. Phys. Chem. A* **2001**, *105*, 3989.

(4) Audier, H. E.; Milliet, A.; Perret, C.; Tabet, J. C.; Varenne, P. *Org. Mass Spectrom.* **1978**, *13*, 315.

(5) Bouchoux, G.; Choret, N.; Flammang, R. *J. Phys. Chem.* **1997**, *101*, 4271.

(6) Holmes, J. L.; Osborne, A. D. *Int. J. Mass Spectrom. Ion Processes* **1977**, *23*, 189.

(7) Bateman, R. H.; Brown, J.; Lefevere, M.; Flammang, R.; Van Haverbeke, Y. *Int. J. Mass Spectrom. Ion Processes* **1992**, *115*, 205.

(8) Frisch, M. J. L.; Trucks, G. W.; Schlegel, H. B.; Gill, M. W.; Johnson, B. G.; Robb, M. A.; Cheeseman, J. R.; Keith, T.; Petersson, G. A.; Montgomery, J. A.; Raghavachari, K.; Al-Laham, M. A.; Zakrzewski, V. G.; Ortiz, J. V.; Foresman, J. B.; Cioslowski, J.; Stefanov, B. B.; Nanayakkari, A.; Challacombe, M.; Peng, C. Y.; Ayala, P. Y.; Chen, W.; Wong, M. W.; Andres, J. L.; Replogle, E. S.; Gomperts, R.; Martin, R. L.; Fox, D. J.; Binkley, J. S.; Defrees, D. J.; Baker, J.; Steward, J. P.; Head-Gordon, M.; Gonzalez, C.; Pople, J. A. *Gaussian 94*, revision C.3; Gaussian, Inc.: Pittsburgh, PA, 1995.

(9) (a) Curtiss, L. A.; Raghavachari, K.; Trucks, G. W.; Pople, J. A. *J. Chem. Phys.* **1991**, *94*, 7221. (b) Curtiss, L. A.; Raghavachari, K.; Pople, J. A. *J. Chem. Phys.* **1993**, *98*, 1293. (c) Curtiss, L. A.; Redfern, P. C.; Smith, B. J.; Radom, L. *J. Chem. Phys.* **1996**, *104*, 5148. (d) Curtiss, L. A.; Raghavachari, K.; Redfern, P. C.; Pople, J. A. *J. Chem. Phys.* **1997**, *106*, 1063. (e) Nicolaides, A.; Rauk, A.; Glukhovtsev, M. N.; Radom, L. *J. Phys. Chem.* **1996**, *100*, 17460.

(10) Pedley, J. B.; Naylor, R. D.; Kirby, S. P. *Thermochemical Data of Organic Compounds*; Chapman & Hall: London, 1986.

(11) Lias, S. G.; Bartmess, J. E.; Liebman, J. F.; Holmes, J. L.; Levin, R. D.; Mallard, W. G. Gas Phase Ion and Neutral Thermochemistry. *J. Phys. Chem. Ref. Data* **1988**, *17*, Suppl. 1.

(12) Hunter, E. P. L.; Lias, S. G. *J. Phys. Chem. Ref. Data* **1998**, *27*, 413.

(13) (a) Mo, O.; de Paz, J. L. G.; Yanez, M. *J. Phys. Chem.* **1987**, *91*, 6484. (b) Barone, V.; Lelj, F.; Grande, P.; Russo, N. *J. Mol. Struct. (THEOCHEM)* **1985**, *124*, 319. (c) Jordan, F. *J. Phys. Chem.* **1976**, *80*, 76. (d) Barone, V.; Lelj, F.; Grande, P.; Russo, N.; Toscano, M. *Chem. Phys. Lett.* **1987**, *133*, 548.

(14) (a) Nixdorf, A.; Grützmacher, H. F. *J. Am. Chem. Soc.* **1997**, *119*, 6544. (b) Audier, H. E.; Milliet, A.; Sozzi, G.; Denhez, J. P. *Org. Mass Spectrom.* **1984**, *19*, 79. (c) Bursey, M. M.; Harvan, D. J.; Parker, C. E.; Darden, T. A.; Hass, J. R. *Org. Mass Spectrom.* **1983**, *18*, 530. (d) Van de Sande, C. C.; Ahmad, S. Z.; Borchers, F.; Levsen, K. *Org. Mass Spectrom.* **1978**, *13*, 666. (e) Levsen, K.; McLafferty, F. W. *J. Am. Chem. Soc.* **1974**, *96*, 139.

(15) (a) Flammang, R.; Gallez, L.; Van Haverbeke, Y.; Wong, M. W.; Wentrup, C. *Rapid Commun. Mass Spectrom.* **1996**, *10*, 232. (b) Aubry, C.; Holmes, J. L. *J. Am. Soc. Mass Spectrom.* **2001**, *12*, 23.

(16) (a) Yamabe, S.; Hirao, K.; Wasada, H. *J. Phys. Chem.* **1992**, *96*, 10261. (b) Ikuta, S.; Nomura, O. *Chem Phys. Lett.* **1989**, *154*, 71.

(17) Benson, S. W. *Thermochemical Kinetics*, 2nd ed.; John Wiley & Sons: New York, 1976.

(18) Frosing, F.; Turecek, F. *J. Am. Soc. Mass Spectrom.* **1998**, *9*, 242.

(19) See, for example: Bouchoux, G.; Choret, N. *Rapid Commun. Mass Spectrom.* **1997**, *11*, 1799 and references therein.